IEEE Access
Multidisciplinary | Rapid Review | Open Access Journal

Received 6 March 2025, accepted 16 April 2025, date of publication 28 April 2025, date of current version 7 May 2025.

Digital Object Identifier 10.1109/ACCESS.2025.3565186

THEORY

Virtual Load Theory: A General Approach for Mitigating Mutual Coupling in Antenna Arrays

MAJID MANTEGHI, (Senior Member, IEEE)
Bradley Department of Electrical and Computer Engineering, Virginia Polytechnic Institute and State University (Virginia Tech), Blacksburg, VA 24060, USA
e-mail: manteghi@vt.edu

ABSTRACT This paper introduces a generalized *Virtual Load Theory* (VLT) for mitigating mutual coupling in antenna arrays through digital signal preprocessing. The method employs Coupling Compensation Matrices (CCMs) derived from generalized Thévenin-Helmholtz equivalent circuits, formulated using impedance and scattering matrices. A key finding reveals that the scattering matrix-based CCM does not always align with the impedance matrix-based solution; this discrepancy is analyzed and resolved to ensure theoretical consistency. Unlike traditional compensation techniques, VLT enables effective coupling mitigation without requiring physical modifications to the array or continuous recalculations. We define two major antenna elements as current-driven (CD), such as a dipole antenna, and voltage-driven (VD), such as a patch antenna. In receiving arrays, we demonstrate that the open-circuit voltage, V_{oc}, for CD elements and short-circuit current, I_{sc}, for VD elements are inherently immune to mutual coupling. Simulation results show that the method successfully recovers embedded element patterns, closely matching isolated patterns even under severe coupling conditions. Experimental validation using a two-monopole prototype array with 0.13λ element spacing further confirms the effectiveness of VLT in eliminating mutual coupling effects in far-field radiation patterns.

INDEX TERMS Antenna arrays, embedded element patterns, active element patterns, mutual coupling, phased arrays.

I. INTRODUCTION

AS wireless communication systems advance toward 5G, 6G, and beyond, antenna arrays play a pivotal role in achieving high data rates, precise beamforming, and efficient spectrum utilization. However, a significant challenge limiting their performance is mutual coupling, which distorts radiation patterns, alters active impedance, and degrades beamforming accuracy [1], [2], [3]. Mutual coupling arises from electromagnetic interactions between closely spaced antenna elements, resulting in undesired impedance variations, increased sidelobe levels, and decreased beamforming precision.

The foundational work by Hansen [4], Mailloux [5], [6], and Stein [7] provided essential insights into mutual coupling phenomena in phased arrays utilized for radar and communication systems. Subsequent theoretical advancements by De Hoop [8], [9] further developed methodologies for analyzing and mitigating mutual coupling through N-port network theory. These early contributions laid the groundwork for addressing mutual coupling in modern applications, such as adaptive arrays and massive MIMO systems for 5G [10].

Over the years, various techniques have been proposed to mitigate mutual coupling and enhance antenna array performance. These include compensation matrices and virtual impedance [11], [12], [13], [14], [15], [16], [17], spatial reconfiguration of elements [18], and the use of electromagnetic bandgap (EBG) structures, metamaterials, and metasurfaces for isolation [19], [20], [21]. Another approach involves integrating parasitic elements [22] or defected ground structures (DGS) [23] to modify the antenna environment and reduce coupling. While these physical techniques can be effective, they introduce several significant drawbacks.

Challenges of Physical Mutual Coupling Mitigation Techniques: Physical solutions, such as EBG structures [19],

The associate editor coordinating the review of this manuscript and approving it for publication was Luyu Zhao.

parasitic elements [22], and DGS-based approaches [23], necessitate modifications to the antenna layout, which increases the overall size, weight, and cost of the system. Moreover, these techniques are often inherently narrowband, which limits their effectiveness across wide frequency ranges. This poses challenges for broadband applications, such as ultra-wideband (UWB) MIMO [24]. Additionally, physical mitigation techniques can negatively impact the antenna's phase response, group delay variation, and overall impedance matching, leading to performance degradation in high-precision beamforming applications [25]. Given these limitations, there is an increasing demand for noninvasive, computationally efficient alternatives.

This paper introduces the general form of *Virtual Load Theory* (VLT), a method designed to mitigate mutual coupling in various antenna configurations without necessitating physical modifications to the array. VLT leverages *Coupling Compensation Matrices* (CCM) [12], [15], [17], [26], [27], [28], [29], [30], [31], derived from impedance or scattering matrices, to preprocess input signals in the digital signal processing (DSP) domain. By simulating physical load conditions through virtual short or open circuits, the method effectively reduces coupling effects without requiring constant recalculation. For receiving arrays, the approach utilizes the open-circuit voltage (V_{oc}), which is inherently immune to mutual coupling, ensuring accurate beamforming and preserving signal integrity.

The proposed framework is validated through theoretical, simulated, and experimental results. Its broad applicability is demonstrated with dipole and microstrip patch antennas, while its scalability is extended to multimode waveguides using a Thévenin-Helmholtz (TH) equivalent circuit. VLT's versatility, along with CCM, makes it highly relevant to modern communication, radar, and sensing applications.

The remainder of the paper is organized as follows: Section II discusses circuit models and driven elements, and Section III presents the theoretical foundations of VLT and its application to transmission lines and waveguides. Section IV details the development of the CCM using TH equivalent circuits. Section V discusses simulation results for various antenna configurations, including dipole and patch arrays, with a focus on $V_{\text{oc}}, (I_{\text{sc}})$-based beamforming for receiving arrays. Section VI presents the measurement results for a prototype system. Finally, Section VII concludes the paper with a discussion of the findings and future research directions.

II. CIRCUIT MODEL AND DRIVEN ELEMENTS

Several factors, including element spacing, surrounding materials, and the types of antenna elements used, can influence the mutual coupling among antenna elements in an array. The effectiveness of any technique for mitigating mutual coupling relies on these factors. Traditional array theory assumes that the current distribution across all antenna elements in an array remains constant, with minimal influence from mutual coupling. However, in situations

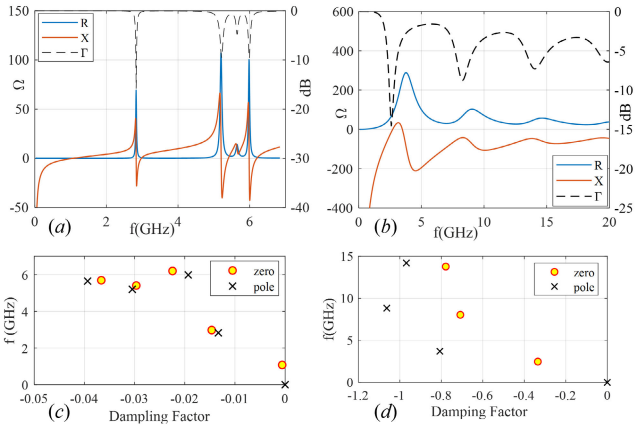

FIGURE 1. Input impedance of common antenna elements in the Laplace domain. (a) Patch antenna impedance. (b) Dipole antenna impedance. (c) Poles and zeros for the patch antenna. (d) Poles and zeros for the dipole antenna.

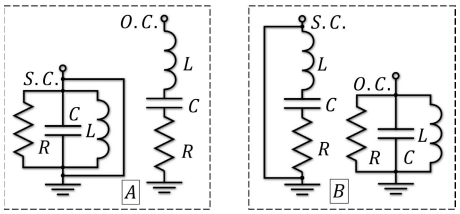

FIGURE 2. Series and parallel resonators with short-circuited and open-circuited terminations.

where mutual coupling is strong, the current distribution across individual antenna elements is altered according to their position within the array. In these cases, conventional array theory is inadequate, requiring a full-wave analysis to accurately capture and characterize the complex interactions and overall behavior of the array.

In our exploration of mutual coupling, we analyzed the input impedance of two commonly used antennas: a dipole antenna and a microstrip patch antenna. The dipole antenna measures 2 inches in length and 50 mils in diameter, while the patch antenna measures 34 mm by 37 mm and is etched on an RT/Duroid®5870 substrate with a thickness of 20 mils and a relative permittivity of $\varepsilon_{\text{r}} = 2.33$. Simulations were conducted using Ansys HFSS, and the resulting input impedances and return losses are presented in Figure 1.

A. INPUT IMPEDANCE AND RESONANCE IN THE LAPLACE DOMAIN

Modeling an antenna's input impedance $Z(s)$ as a Laplace-domain transfer function elucidates its resonant characteristics, akin to passive network analysis where impedance is defined by poles and zeros. For a passive, linear, time-invariant (LTI) system, $Z(s)$ can be expressed as:

$$Z(s) = Z_0 \frac{\prod_{l=1}^{L}(s+p_l)\prod_{j=1}^{M}\left(s^2+2\zeta_j\omega_j s+\omega_j^2\right)}{\prod_{k=1}^{K}(s+z_k)\prod_{i=1}^{N}\left(s^2+2\zeta_i\omega_i s+\omega_i^2\right)} \quad (1)$$

Here, Z_0 is a scaling factor with units of ohms (Ω). Linear terms represent first order poles and zeros; quadratic terms denote complex conjugate pairs with damping ratio ζ and natural frequency ω. Complex conjugate zeros correspond to series resonances (impedance minima), and poles to parallel resonances (impedance maxima). A pole at the origin indicates infinite impedance at DC, characteristic of antennas like dipoles and microstrip patches.

The impedance function must be positive-real (PR), ensuring passivity and causality. Consequently, poles and zeros alternate along the frequency axis—a property inherent to PR functions.

B. VOLTAGE-DRIVEN (VD) AND CURRENT-DRIVEN (CD) ANTENNAS

In the microstrip patch antenna, the first pair of zeros arises ($-0.001 \pm 1.0794j\ GHz$) due to the static capacitance between the patch and the ground plane resonating with the parasitic inductance of the feeding probe, forming a series resonance (Figure 1 (a) and (c)). However, this mode does not radiate efficiently. The first significant radiating mode, associated with the poles ($-0.0133 \pm 2.829\ GHz$), is modeled by a parallel resonator, which defines the operational frequency of the antenna. Higher-order radiating modes of the patch antenna are linked to higher-order poles.

In contrast, the dipole antenna exhibits a series resonance in the first pair of zeros, representing its primary radiation mode ($-0.335 \pm 2.47j\ GHz$). Return loss indicates that higher-order radiating modes are associated with the zeros of the input impedance, which is characteristic of series resonance behavior (Figures 1 (b) and (d)). This characteristic behavior classifies dipoles as current-driven (CD) antennas. Antennas such as microstrip patches, where a parallel resonator models the primary radiation mode, are considered voltage-driven (VD) antennas. The distinction between CD and VD antennas underlines the fundamental differences in their excitation and resonance mechanisms.

C. RESONATOR ANALYSIS AND MUTUAL COUPLING MITIGATION

Understanding the distinction between VD and CD antennas is crucial for optimizing excitation coefficients in antenna arrays. Figure 2 illustrates different terminations of series and parallel resonators. Group A resonators are considered null due to the absence of resonance, while Group B resonators can still support damped oscillations. Terminating CD antennas to open circuits and VD antennas to short circuits terminates their resonance for the specific set of zeros and poles, respectively. Nulling these antennas from mutual coupling is achieved by making them behave as open/short circuits at the resonance port, isolating themselves from mutual coupling effects. The goal is to virtually nullify the resonant antennas to eliminate excitations caused by mutual coupling, making the antennas immune to mutual coupling.

We define the resonance port as the point on the antenna where a short or open circuit can be directly connected to the antenna's impedance poles or zeros. Locating resonant ports in practical applications often presents challenges due to parasitic elements (see Figure 3). Deembedding is necessary to establish ideal conditions at the resonance port, ensuring effective decoupling and minimizing the influence of mutual coupling. On a positive note, de-embedding parameters of one element provide a very good approximation for all elements in the array.

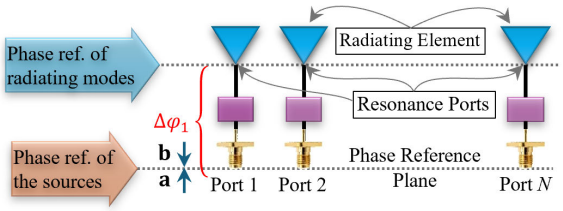

FIGURE 3. Representation of resonance and antenna ports. The feeding structure must be de-embedded to properly relate the resonance port to the antenna port.

III. VIRTUAL LOAD THEORY

In order to minimize mutual coupling between antenna elements in arrays, it is crucial to utilize virtual short or open circuits by adjusting the array's excitation coefficients. Before delving into specific techniques for interference reduction, it is essential to establish the theoretical foundation for virtual loading a transmission line. This foundation will demonstrate that virtual load theory is not confined to circuit-level analysis but is deeply rooted in fundamental electromagnetic theorems, such as 'Huygens Principle and the surface equivalence theorem. This section commences with an examination of a TEM transmission line terminated with a complex load impedance, elucidating the basic principles of virtual loading. The theory is then extended to encompass more general waveguide configurations, providing a comprehensive framework that applies to a wider range of practical antenna systems.

A. VIRTUAL LOAD ON TRANSMISSION LINES

Consider a TEM transmission line with characteristic impedance Z_0, terminated by a complex load impedance Z_L, as illustrated in Figure 4 (a). The voltage and current reflected from the load can be expressed using the reflection coefficient:

$$V^- = \Gamma V^+, \quad I^- = -\frac{\Gamma V^+}{Z_0}, \quad \Gamma = \frac{Z_L - Z_0}{Z_L + Z_0} \tag{2}$$

In the provided configuration, V^+ and V^- represent the forward and reflected voltage waves, respectively, while Γ is the reflection coefficient. We can substitute Z_L with an auxiliary source V_1 (Figure 4b) with source impedance Z_0 as:

$$V_1 = 2V^-(L) = 2\Gamma V^+ \tag{3}$$

In this arrangement, the voltage and current distributions along the line remain unchanged, and the voltage source V_1

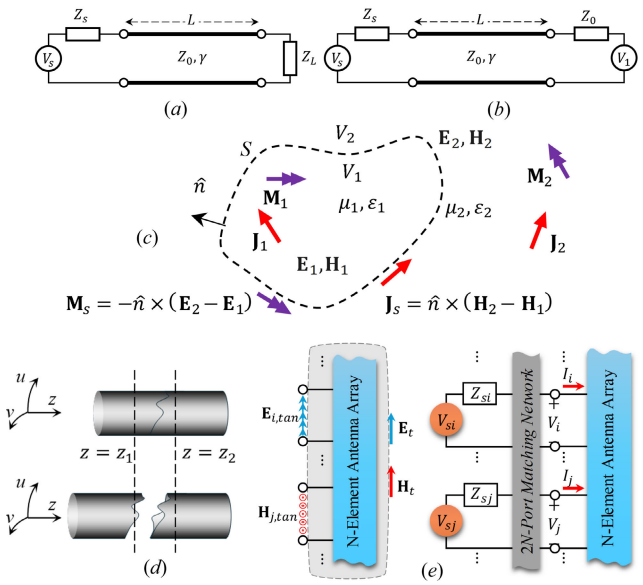

FIGURE 4. (a) Source-load connection via a transmission line. (b)One-dimensional equivalence theorem with source V_1 and impedanceZ_0 (c) Surface equivalence principle with sources and fields indistinct media. (d) Waveguide supporting multiple modes at across-section. (e) N-port network showing tangential electric andmagnetic fields, voltages, and currents.

with its source impedance Z_0 effectively acts as a load Z_L to an observer along the transmission line. By adjusting the phase of V_1, the virtual load can be positioned anywhere along the line—an application of the Equivalence Principle.

B. THEORETICAL FOUNDATION VIA EQUIVALENCE PRINCIPLE

The foundation of Virtual Load Theory (VLT) is rooted in the Surface Equivalence Principle [32], [33]. Consider the electromagnetic fields and sources $(\mathbf{E}_1, \mathbf{H}_1, \mathbf{J}_1, \mathbf{M}_1)$ in medium 1 characterized by $(\mu_1, \varepsilon_1, \sigma_1)$ that satisfy Maxwell's equations. Similarly, the fields and sources $(\mathbf{E}_2, \mathbf{H}_2, \mathbf{J}_2, \mathbf{M}_2)$ in medium 2, characterized by $(\mu_2, \varepsilon_2, \sigma_2)$, also independently satisfy Maxwell's equations. Now, let the source-free region of medium 2 be enclosed by an arbitrary surface S, which contains $(\mathbf{J}_1, \mathbf{M}_1)$, be replaced by the medium 1 material. The Surface Equivalence Principle states that the fields inside S (now in medium 1) and the fields outside S (remaining in medium 2) will remain unchanged if the following surface currents are applied on S:

$$\mathbf{J}_s = \hat{n} \times (\mathbf{H}_2 - \mathbf{H}_1), \quad \mathbf{M}_s = \hat{n} \times (\mathbf{E}_1 - \mathbf{E}_2) \tag{4}$$

where $\hat{n}$ is the normal vector to the surface S. The Uniqueness Theorem guarantees this equivalence, ensuring that the external fields will be identical as long as the boundary conditions are satisfied.

An additional step is necessary to derive the Virtual Load Theory (VLT) from the surface equivalent principle. The direct application of the equivalence principle requires the inclusion of both electric and magnetic surface currents (currents and voltages in circuits with lumped elements). In the following section, we will refine this principle to make it applicable to a general transmission line, particularly a multimode arbitrary cross-sectional waveguide.

C. APPLICATION TO ARBITRARY WAVEGUIDE CONFIGURATIONS

Let us consider a waveguide with an arbitrary cross-section at the port i of a network, as depicted in Figure 4(d). The electromagnetic fields inside the waveguide can be decomposed into a set of orthogonal modes, with each mode propagating in either the positive or negative longitudinal direction. This principle applies even to inhomogeneous waveguides, provided that the appropriate inner product is defined. The total electric and magnetic fields $\mathbf{E}(u, v, z)$ and $\mathbf{H}(u, v, z)$ within the waveguide are expressed as sums of forward and backward propagating modes [34]:

$$\begin{cases} \mathbf{E}(u,v,z) = \sum_m \left(A_m^+ \mathbf{E}_m^+(u,v,z) + A_m^- \mathbf{E}_m^-(u,v,z) \right) \\ \mathbf{H}(u,v,z) = \sum_m \left(A_m^+ \mathbf{H}_m^+(u,v,z) - A_m^- \mathbf{H}_m^-(u,v,z) \right) \end{cases} \tag{5}$$

Here, β_m is the propagation constant for the m-th mode, and $\mathbf{E}_m^{\pm}(u, v, z)$ and $\mathbf{H}_m^{\pm}(u, v, z)$ represent the electric and magnetic fields propagating in positive and negative directions for the corresponding modes as:

$$\begin{cases} \mathbf{E}_m^+(u,v,z) = (\mathbf{e}_m(u,v) + \mathbf{e}_{zm}(u,v)) e^{-j\beta_m z} \\ \mathbf{H}_m^+(u,v,z) = (\mathbf{h}_m(u,v) + \mathbf{h}_{zm}(u,v)) e^{-j\beta_m z} \\ \mathbf{E}_m^-(u,v,z) = (\mathbf{e}_m(u,v) - \mathbf{e}_{zm}(u,v)) e^{j\beta_m z} \\ \mathbf{H}_m^-(u,v,z) = (\mathbf{h}_m(u,v) - \mathbf{h}_{zm}(u,v)) e^{j\beta_m z} \end{cases} \tag{6}$$

where $\mathbf{e}_m, \mathbf{e}_{zm}, \mathbf{h}_m$, and $\mathbf{h}_{zm}$ are transverse and longitudinal components of the electric field and magnetic fields for the m-th mode. The transverse components of electric and magnetic fields for each mode are related as $Z_m \mathbf{h}_m = \hat{z} \times \mathbf{e}_m$ where Zm is impedance of the mth mode. The tangential electric and magnetic fields on an arbitrary cross-section S can be decomposed as the summation of waveguide modes as:

$$\begin{aligned} \mathbf{E}_{\tan}(u,v,z) &= \left(\bar{\bar{\mathbf{I}}} - \hat{n}\hat{n} \right) \cdot \mathbf{E}(u,v,z), \\ \mathbf{H}_{\tan}(u,v,z) &= \left(\bar{\bar{\mathbf{I}}} - \hat{n}\hat{n} \right) \cdot \mathbf{H}(u,v,z) \end{aligned} \tag{7}$$

Here, $\hat{n}$ is the normal vector for the cross section S, and $(\bar{\bar{\mathbf{I}}} - \hat{n}\hat{n})$ extracts the tangential components of the fields. According to the Surface Equivalence Principle, the electromagnetic fields for $z > z_2$ remain unchanged as long as the tangential electric and magnetic fields on S satisfy the above equations, even if the waveguide beyond S is altered or removed. In this formulation, the coefficients A_m^+ represent the modal excitations.

Once the tangential electric field, $\mathbf{E}_{\tan}(u, v, z)$, or the magnetic field, $\mathbf{H}_{\tan}(u, v, z)$, on the cross-section is known (A_m^+ are for every m), the backward-propagating modal coefficients, A_m^-, can be determined using the orthogonality of the waveguide modes. These coefficients completely define the reflected wave in the waveguide. This implies that

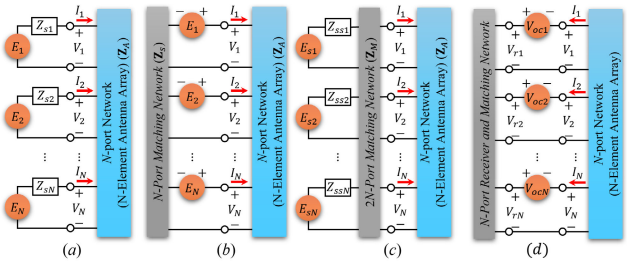

FIGURE 5. (a) Sources with isolated impedance networks. (b) Sources with interconnected feeding networks. (c) Sources and antenna array via a2N-port matching circuit. (d) The general form of an antenna array in receiving mode is connected to a multiport receiver.

only the tangential components of one field, either electric or magnetic, are required to synthesize the reflected wave, guaranteeing that the virtual load behaves in the same way as a physical load for the external observer.

With the foundation of mode-based waveguide analysis established, we nowbintroduce the formal definition of Virtual Load Theory (VLT). VLT posits that any load in an LTI transmission line or waveguide can be effectively realized at any point along the line by generating a reflected voltage or current (or, equivalently, the electric or magnetic fields) identical to those produced by a physical load. In essence, the virtual load behaves exactly like the physical load concerning the reflected fields, while offering greater flexibility in load positioning and control.

Leveraging circuit theory in the context of waveguides allows us to calculate the equivalent voltages and currents [34] for both the electric and magnetic fields. This approach allows us to construct a matrix-based representation for any N-port network, as depicted in Figure 4(e), which generalizes transmission lines to more complex waveguide systems. The matrix formulation enables the determination and application of virtual loads to the excitation coefficients of an array, ensuring that the desired reflection and transmission characteristics are achieved while compensating for the effects of mutual coupling.

This generalized application of VLT extends its utility to multi-mode waveguides, antenna arrays, and other complex transmission systems, making it a robust tool for controlling wave propagation and field interactions in diverse electromagnetic environments.

IV. COUPLING COMPENSATION MATRIX, CCM, AND THÉVENIN-HELMHOLTZ'S EQUIVALENT CIRCUIT

In this section, we further refine the derivation of the CCM [7], [12], [15], [17], [27], [29], [30] for specific terminations: short and open circuits correspond to voltage-driven (VD) and current-driven (CD) antennas. Although mutual coupling originates as a field phenomenon, it can be addressed purely as a circuit model when analyzed with network parameters. Therefore, the treatment presented here focuses on circuit parameters and network analysis. The derivation utilizes the generalized TH equivalent circuit approach, assuming that the antenna type (VD or CD) remains consistent within the frequency range of interest. This approach is extendable to multimode and multipolarization antennas, considering that all modes exhibit consistent detuning characteristics under short-circuit and open-circuit conditions.

The CCM prepares the array coefficients for input into the antenna array, which is typically performed in the frequency domain within the Digital Signal Processing (DSP) unit. Applying the CCM aligns the coefficients with their desired values, compensating for mutual coupling effects and effectively mitigating coupling impacts within the array. We also explore different definitions of the CCM derived from impedance and scattering matrices, highlighting their similarities and differences.

A. GENERALIZED THÉVENIN-HELMHOLTZ THEOREM

Figure 5 depicts three equivalent circuit models for a transmitter and receiver front-end system connected to an N-element antenna array. The TH equations for the general form of the transmitting array (the receiving array will be studied separately), shown in Figure 5, are given as follows:

$$\mathbf{V} = \mathbf{E} - \mathbf{Z}_\mathrm{s}\mathbf{I}, \quad \text{where} \quad \mathbf{V} = \mathbf{Z}\mathbf{I} \tag{8}$$

In this equation, $\mathbf{Z}_\mathrm{s}$ represents the source impedance, $\mathbf{E}$ is the vector of input voltages, and $\mathbf{I}$ is the vector of currents.

In Figure 5 (a), the impedance matrix of the source is diagonal, indicating that each source is independent and isolated from the others. In Figure 5(b), the source impedance matrix can be non-diagonal, implying coupling between sources, which suggests interconnections between the array elements. Figure 5(c) introduces a matching network, where the 2N-by-2N impedance matrix is decomposed into four distinct N-by-N matrices: ($\mathbf{Z}_\mathrm{in}$, $\mathbf{Z}_\mathrm{io}$, $\mathbf{Z}_\mathrm{oi}$, $\mathbf{Z}_\mathrm{out}$). This decomposition allows us to represent the source-network connection in the standard HT form:

$$\mathbf{Z}_{2\mathrm{N}} = \begin{bmatrix} \mathbf{Z}_\mathrm{in} & \mathbf{Z}_\mathrm{io} \\ \mathbf{Z}_\mathrm{oi} & \mathbf{Z}_\mathrm{out} \end{bmatrix}, \begin{cases} \mathbf{Z}_\mathrm{s} = \mathbf{Z}_\mathrm{out} - \mathbf{Z}_\mathrm{oi}(\mathbf{Z}_\mathrm{in} + \mathbf{Z}_\mathrm{ss})^{-1}\mathbf{Z}_\mathrm{io} \\ \mathbf{E} = \mathbf{Z}_\mathrm{oi}(\mathbf{Z}_\mathrm{in} + \mathbf{Z}_\mathrm{ss})^{-1}\mathbf{E}_\mathrm{s} \end{cases} \tag{9}$$

This equation enables us to utilize the TH equations for the general case of a connection between a source network and the N-element array.

B. TRANSMITTER

The input impedances of ideal voltage and current sources are zero and infinity, respectively. Thus, these sources can be utilized effectively for voltage-driven VD and current-driven CD antennas to serve as both sources and virtual loads. On the transmitter side, we can rearrange the TH equations to relate the input voltage sources $\mathbf{E}$ to the actual array voltage $\mathbf{V}$ and current $\mathbf{I}$ as follows:

$$\mathbf{E} = (\mathbf{Z} + \mathbf{Z}_\mathrm{s})\,\mathbf{I}, \qquad \mathbf{E} = (\mathbf{Z} + \mathbf{Z}_\mathrm{s})\,\mathbf{Z}^{-1}\mathbf{V} \tag{10}$$

Equation (10) enables us to determine the required set of excitation $\mathbf{E}$ to provide any arbitrary set of currents ($\mathbf{I}$) or

voltages ($\mathbf{V}$) at the ports of the antenna array. From these expressions, we derive the CCM for CD and VD antenna elements:

$$\mathbf{C}_{\mathrm{o}} = (\mathbf{Z}+\mathbf{Z}_{\mathrm{s}}), \qquad \mathbf{C}_{\mathrm{s}} = (\mathbf{Z}+\mathbf{Z}_{\mathrm{s}})\,\mathbf{Z}^{-1} \tag{11}$$

Here, C_{s} is the CCM for VD antennas and C_{o} is for CD antennas. *Normalization is necessary* to make the matrices dimensionless by dividing each row by its diagonal element, ensuring the diagonal elements equal 1.

C. SCATTERING MATRIX AND VIRTUAL CIRCUITS

The scattering matrix, $\mathbf{S}$, can also simulate virtual short circuits and open circuits at the antenna ports. In the case of a virtual short circuit, the scattered signal mirrors the incident signal with a 180-degree phase shift, that is, $\mathbf{b_s} = -\mathbf{a_s}$. For a virtual open circuit, the scattered signal equals the incident signal, i.e. $\mathbf{b_o} = \mathbf{a_o}$. The total reflected signal is calculated as follows:

$$\mathbf{b}_{\mathrm{s}} = (\mathbf{U}+\mathbf{S})\,\mathbf{a}_{\mathrm{s}}, \qquad \mathbf{b}_{\mathrm{o}} = (\mathbf{U}-\mathbf{S})\,\mathbf{a}_{\mathrm{o}} \tag{12}$$

Thus, the CCMs for short-circuit and open-circuit conditions at the transmitter are as follows:

$$\mathbf{c}_{\mathrm{s}} = (\mathbf{U}+\mathbf{S})^{-1}, \qquad \mathbf{c}_{\mathrm{o}} = (\mathbf{U}-\mathbf{S})^{-1} \tag{13}$$

Here, uppercase C represents impedance-based CCMs, while lowercase $\mathbf{c}$ represents CCMs based on scattering matrix. To compare these, we use the generalized scattering matrix [35] for power waves:

$$\begin{aligned} \mathbf{S} &= \mathbf{R}_{\mathrm{s}}^{-1/2}\left(\mathbf{Z}-\mathbf{Z}_{\mathrm{s}}^{H}\right)(\mathbf{Z}+\mathbf{Z}_{\mathrm{s}})^{-1}\,\mathbf{R}_{\mathrm{s}}{}^{1/2} \\ \mathbf{R}_{\mathrm{s}} &= \mathrm{Re}\,(\mathbf{Z}_{\mathrm{s}}) \end{aligned} \tag{14}$$

Let us use the following equivalence for the unity matrix:

$$\mathbf{U} = \mathbf{R}_{\mathrm{s}}^{-1/2}\,(\mathbf{Z}+\mathbf{Z}_{\mathrm{s}})\,(\mathbf{Z}+\mathbf{Z}_{\mathrm{s}})^{-1}\,\mathbf{R}_{\mathrm{s}}^{1/2} \tag{15}$$

Substituting into the previous expressions for $\mathbf{c}_{\mathrm{s}}$ and $\mathbf{c}_{\mathrm{o}}$, gives:

$$\begin{aligned} \mathbf{U}\pm\mathbf{S} = \mathbf{R}_{\mathrm{s}}^{-1/2}\Big[(\mathbf{Z}+\mathbf{Z}_{\mathrm{s}}) \pm \left(\mathbf{Z}-\mathbf{Z}_{\mathrm{s}}^{H}\right)\Big] \\ \times\,(\mathbf{Z}+\mathbf{Z}_{\mathrm{s}})^{-1}\,\mathbf{R}_{\mathrm{s}}^{1/2}. \end{aligned} \tag{16}$$

This simplifies to the following equations:

$$\mathbf{c}_{\mathrm{s}} = \frac{1}{2}\mathbf{R}_{\mathrm{s}}^{-1/2}\,(\mathbf{Z}+\mathbf{Z}_{\mathrm{s}})\,(\mathbf{Z}+j\mathrm{Im}\,(\mathbf{Z}_{\mathrm{s}}))^{-1}\,\mathbf{R}_{\mathrm{s}}^{1/2} \tag{17}$$

$$\mathbf{c}_{\mathrm{o}} = \frac{1}{2}\mathbf{R}_{\mathrm{s}}^{-1/2}\,(\mathbf{Z}+\mathbf{Z}_{\mathrm{s}})\,\mathbf{R}_{\mathrm{s}}^{-1/2} \tag{18}$$

As with impedance-based CCMs, these matrices must also be normalized by their diagonal elements to ensure that they are dimensionless. The CCMs derived from impedance matrices ($\mathbf{C}_{\mathrm{s}}$, $\mathbf{C}_{\mathrm{o}}$) and those from the scattering matrix ($\mathbf{c}_{\mathrm{s}}$, $\mathbf{c}_{\mathrm{o}}$), are identical when $\mathbf{Z}_{\mathrm{s}} = Z_0\mathbf{U}$ and $\mathrm{Im}(Z_0) = 0$.

D. RECEIVER

Figure 5 (d) depicts a receiving antenna array connected to a multiport receiver. Each antenna element is modeled as a voltage source (open-circuit voltage) in series with its corresponding port in the N-port network, representing the antenna array in receiving mode. This figure illustrates the general Thévenin-Helmholtz (TH) equivalent network for an N-element antenna array connected to an N-port receiver:

$$\mathbf{V}_{\mathrm{r}} = \mathbf{Z}_{\mathrm{r}}\mathbf{I}, \quad \mathbf{V} = -\mathbf{Z}\mathbf{I}. \tag{19}$$

In the receiver configuration, the quantities $\mathbf{V}_{\mathrm{r}}$ (or $\mathbf{I}_{\mathrm{r}}$), $\mathbf{Z}_{\mathrm{r}}$, and the impedance matrix of the antenna array $\mathbf{Z}$ are assumed to be known. The goal is to determine $\mathbf{V}$ (or $\mathbf{I}$) from the given $\mathbf{V}_{\mathrm{r}}$ (or $\mathbf{I}_{\mathrm{r}}$). The TH equations governing these relationships are:

$$\mathbf{I} = \mathbf{Z}_{\mathrm{r}}^{-1}\mathbf{V}_{\mathrm{r}}, \qquad \mathbf{V} = -\mathbf{Z}\mathbf{Z}_{\mathrm{r}}^{-1}\mathbf{V}_{\mathrm{r}} \tag{20}$$

As discussed in Section II, the open-circuit voltage $V_{\mathrm{oc,n}}$ in current-driven (CD) antennas and the short-circuit current $I_{\mathrm{sc,n}}$ in voltage-driven (VD) antennas (Norton equivalent network) are unaffected by mutual coupling, with their magnitudes being identical across all array elements. Consequently, receiver beamforming can be performed using $\mathbf{V}_{\mathrm{oc}}$ for CD arrays or $\mathbf{I}_{\mathrm{sc}} = \mathbf{Z}^{-1}\mathbf{V}_{\mathrm{oc}}$ for VD arrays. The open-circuit voltage and short-circuit current can be determined from Figure 5 (d) using the following system of equations:

$$\begin{cases} \mathbf{V}_{\mathrm{oc}} &= (\mathbf{Z}_{\mathrm{r}}+\mathbf{Z})\,\mathbf{I}_{\mathrm{r}} \\ \mathbf{I}_{\mathrm{sc}} &= \left(\mathbf{Z}^{-1}\mathbf{Z}_{\mathrm{r}}+\mathbf{U}\right)\mathbf{I}_{\mathrm{r}} \end{cases} \quad \begin{cases} \mathbf{V}_{\mathrm{oc}} &= \left(\mathbf{U}+\mathbf{Z}\mathbf{Z}_{\mathrm{r}}^{-1}\right)\mathbf{V}_{\mathrm{r}} \\ \mathbf{I}_{\mathrm{sc}} &= \left(\mathbf{Z}_{\mathrm{r}}^{-1}+\mathbf{Z}^{-1}\right)\mathbf{V}_{\mathrm{r}} \end{cases} \tag{21}$$

For the n^{th} element, the open-circuit voltage $V_{\mathrm{oc,n}}$ is given by:

$$V_{\mathrm{oc,n}} = \mathbf{E}_{\mathrm{n}}^{i}\cdot\mathbf{l}_{\mathrm{eff,n}} = A_{\mathrm{n}}\mathbf{E}^{0}\cdot\mathbf{l}_{\mathrm{eff,n}}, \quad A_{\mathrm{n}} = e^{jk\hat{r}\cdot\mathbf{r}_{\mathrm{n}}} \tag{22}$$

where $\mathbf{E}_{\mathrm{n}}^{i}$ is the incident electric field, $\mathbf{l}_{\mathrm{eff,n}}$ is the effective length, and $\mathbf{r}_{\mathrm{n}}$ represents the position of the n^{th} element relative to a reference coordinate system. Additionally, $\mathbf{E}_{\mathrm{n}}^{0}$ is the incident field at the origin, and $\hat{r}$ is the unit vector pointing toward the transmitter.

Since $\hat{r}$ depends on θ and φ, any parameter that depends on $\hat{r}$ is also a function of θ and φ. In an array of CD antenna elements, an open circuit leads to uncoupled antennas. Because the current distribution across all antenna elements is identical, differing only by a complex scaling coefficient (which has a magnitude of 1 for CD antennas), we have:

$$\left|V_{\mathrm{oc,n}}\right| = \left|A_{\mathrm{n}}\mathbf{E}^{0}\cdot\mathbf{l}_{\mathrm{eff}}\right| = \left|V_{\mathrm{oc}}\right| \tag{23}$$

Since $|A_{\mathrm{n}}| = 1$, the magnitude of the open circuit voltage $\left|V_{\mathrm{oc,n}}\right|$ for CD antennas remains identical across all antenna elements for a given θ, φ, and is unaffected by mutual coupling. Thus, the array open-circuit voltage vector can be expressed as:

$$\mathbf{V}_{\mathrm{oc}} = V_{\mathrm{oc}}\mathbf{A} \tag{24}$$

Note that $\mathbf{I}_{\mathrm{r}} = \mathbf{I}$. The received signal from a desired direction $\hat{r}_{\mathrm{d}}$ can be obtained using a set of beamforming

coefficients b_n. The received signal V_{rec} for a CD antenna array in the direction of $\hat{r}$ is given by:

$$\mathbf{V}_{rec} = \mathbf{B} \cdot \mathbf{V}_{oc} = V_{oc}\mathbf{B} \cdot \mathbf{A}, \quad B_n = b_n e^{-jk\hat{r}_d \cdot \mathbf{r}_n} \tag{25}$$

Using (22) and (25), V_{rec} is give as:

$$V_{rec} = V_{oc} \sum_{n=1}^{N} b_n e^{jk(\hat{r}-\hat{r}_d)\cdot \mathbf{r}_n} \tag{26}$$

Using the same method, the received current I_{rec} for VD antenna arrays is given by:

$$I_{rec} = I_{sc} \sum_{n=1}^{N} b_n e^{jk(\hat{r}-\hat{r}_d)\cdot \mathbf{r}_n} \tag{27}$$

Equations (26) and (27) represent simple array factors with the desired beamforming coefficients, $\mathbf{B}$, multiplied by V_{oc} or I_{sc}. By applying appropriate beamforming coefficients, the effects of mutual coupling on V_{rec} in CD antennas and I_{rec} in VD antennas can be mitigated, improving signal reception from the intended direction.

V. SIMULATION RESULTS

To validate the effectiveness of the proposed technique, simulations were conducted on two types of antenna arrays: resonant dipole/monopole arrays and microstrip patch antenna arrays. The initial simulations focused on two-element arrays to provide a controlled environment for analyzing mutual coupling behavior and assessing the impact of Virtual Load Theory (VLT). These smaller arrays allowed us to validate the core principles of the technique and compare the simulation results with the experimental data.

Furthermore, larger arrays of microstrip patch antennas and resonant dipoles were simulated to evaluate the proposed method's scalability. The results demonstrated that VLT effectively mitigates mutual coupling and enhances Embedded Element Patterns, EEPs, across various array sizes, making it suitable for small- and large-scale antenna systems. These simulations provide a comprehensive overview of the adaptability of VLT to complex configurations, ensuring consistent performance under diverse operational conditions.

A. EVALUATION METHODOLOGY

For each type of array, we evaluated the proposed coupling compensation technique using the following three cases.

1. The complete array with all antenna elements terminated to their matched loads and only one element excited.
2. The full array, where the other elements are excited using the coefficients derived from the equations presented in Section IV to compensate for mutual coupling.
3. Only the element of interest is present, and all other antenna elements are physically removed.

These three cases serve as a consistent framework for assessing the performance of Virtual Load Theory (VLT) and CCM in mitigating mutual coupling and restoring desired EEPs.

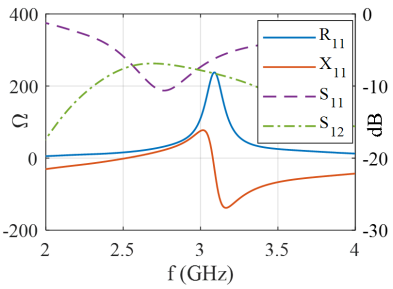

FIGURE 6. Input impedance and scattering parameters of the two-element monopole antenna.

B. DIPOLE ARRAY

The first example considers a two-element monopole antenna array placed on a circular ground plane. The monopoles are 1.0875 inch long and 50 mil in diameter, resulting in a resonance frequency of 2.71 GHz. The ground plane has a radius of 6.75 inches, and the element spacing is 15.9 mm (0.15λ). This small spacing was intentionally chosen to emphasize mutual coupling effects (measured at −6.9 dB), significantly impacting EEPs.

The array was simulated using ANSYS HFSS, and the complex impedance parameters z_{11} and the scattering parameters (s_{11}, s_{12}) in dB scale are presented in Figure 6. The simulated impedance matrix at resonance is:

$$z_{11} = 26.6 + j15.5, \quad z_{12} = 14.2 - j28.2\Omega \tag{28}$$

After normalizing either $\mathbf{c}_o$ or $\mathbf{C}_o$ to the coefficient of Port 1 (or Port 2), the (voltage) compensation coefficient for the other port is calculated as $C_{11} = 1, C_{12} = 0.1064 + j0.39104$. As discussed in Section II, the effect of the SMA connector in the simulation model must be de-embedded to reflect the array performance accurately. After de-embedding, the compensation coefficient (Note that the *power* coefficients used in the HFSS simulation) becomes:

$$c = 0.1637\angle -4 \tag{29}$$

Figure 7 shows the radiation patterns and current distributions on the ground plane for three distinct cases. Specifically, Figure 7 (a, d) shows the results for case 1, Figure 7 (b, e) illustrates the results for case 2, and Figure 7 (c, f) represents case 3.

Upon comparison, it is evident that the coupling-compensated case (Figure 7 (b, e)) closely resembles the scenario in which the second antenna is physically removed (Figure 7 (c, f)). Observing the current distribution on the ground plane for all three cases shows that the ground plane current is significantly altered in case 2 (Figure 7 (e)) and closely resembles the current distribution in case 3 (Figure 7 (f)), highlighting the effect of the VLT on the reactive near-field of the antenna. Note that the offset of the monopole from the center of the ground plane results in an asymmetric radiation pattern, even in the single-element scenario (Figure 7 (c)).

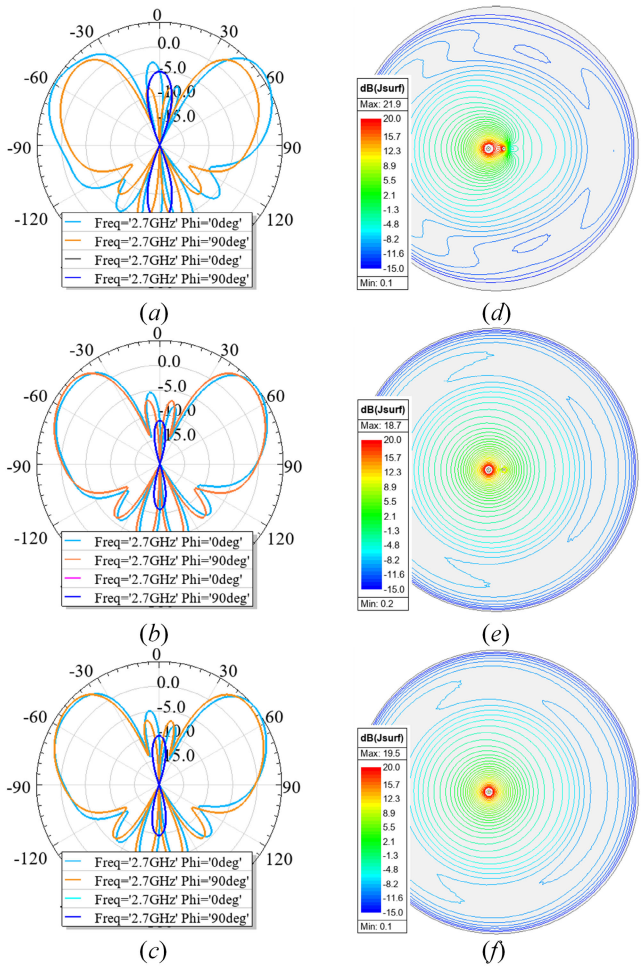

FIGURE 7. Simulation results of the two-element monopole array, showing radiation patterns (a–c) and current distribution on the antennas (Jsurf2) and ground plane (Jsurf) (d–f) for three cases: (a, d) non-compensated array, (b, e) compensated array, and (c, f) single-element array.

The following example involves a closely spaced array of five dipole antennas, each with a diameter of 50 mil and a length of 2 inches. The antennas are placed in a non-griddable arrangement with a minimum spacing between elements of 0.16λ. The location matrix is as follows:

$$\mathbf{P}(mm) = \begin{bmatrix} \mathbf{X} \\ \mathbf{Y} \\ \mathbf{Z} \end{bmatrix} = \begin{bmatrix} 5 & 0 & 20 & -10 & -20 \\ 20 & 0 & 10 & -15 & 20 \\ 0 & 0 & 0 & 0 & 0 \end{bmatrix} \tag{30}$$

The HFSS simulation was used to compute the $\mathbf{Z}$ and $\mathbf{S}$ matrices for the array. The CCM for the open-circuit scenario, denoted as $\mathbf{c}_o$ or $\mathbf{C}_o$, was subsequently calculated and applied to the array. This ensured that Antenna 2 (the center element) was excited while all other elements remained virtually open-circuit. Antenna 2 was selected as the worst-case scenario due to its shortest distances to the surrounding antenna elements. The simulated radiation patterns and current distributions of the dipole array—both with and without coupling compensation, assuming only

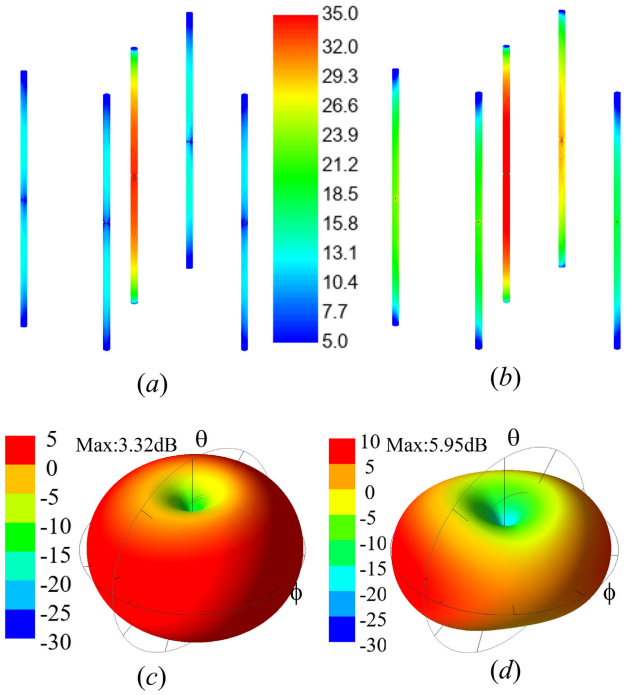

FIGURE 8. Simulation of the closely spaced 5-element dipole array with the center element excited, with and without mutual coupling compensation. (a) Current distribution with compensation. (b) Current distribution without compensation. (c) Directivity pattern with compensation. (d) Directivity pattern without compensation.

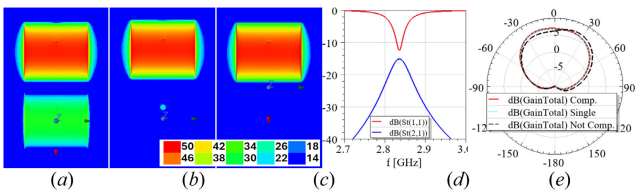

FIGURE 9. (a) Current distribution of the two-patch antenna array in the E-plane (Case 1). (b) Current distribution (Case 2). (c) Currentdistribution (Case 3). (d) Scattering parameters of the array. (e)E-plane radiation patterns for all three cases.

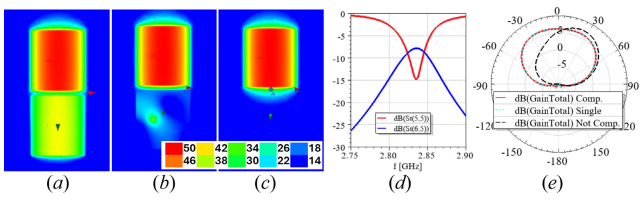

FIGURE 10. (a) Current distribution of the two-patch antenna array in theH-plane (Case 1). (b) Current distribution (Case 2). (c) Currentdistribution (Case 3). (d) Scattering parameters of the array. (e)H-plane radiation patterns for all three.

Element 2 is excited—are presented in Figure 8. The results show that applying VLT and the appropriate coupling compensation significantly mitigates the mutual coupling effects, resulting in radiation patterns similar to those of an isolated element. This verifies the validity of the VLT and

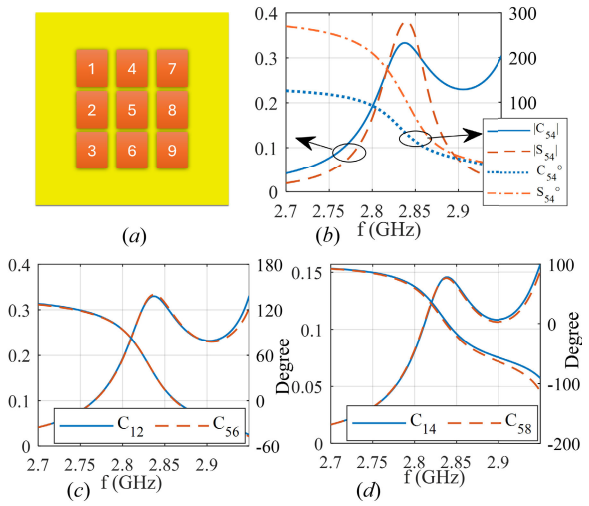

FIGURE 11. (a) Numbering of antenna elements. (b) Phase and magnitude comparison between the S-matrix and the CCM, illustrating the reduced sensitivity of CCM elements to frequency variation. (c, d) Magnitude and phase of CCM elements for antenna pairs with similar relative positions, demonstrating consistency across the frequency range.

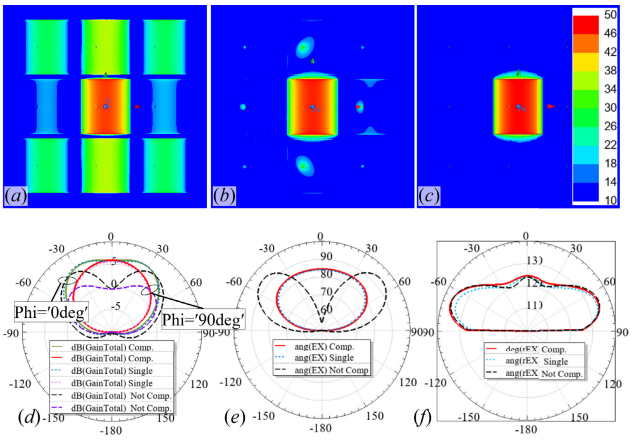

FIGURE 12. (a) Current distribution of the 9-element patch array with thecenter element excited (Case 1). (b) Current distribution (Case 2). (c)Current distribution (Case 3). (d) E-plane and H-plane radiationpatterns for all three cases. (e) Phase of the co-polarized radiated field in the E-plane. (f) Phase of the co-polarized radiated field in the H-plane.

the effectiveness of the CCM in enhancing the EEPs, even in densely packed arrays.

C. PATCH ARRAY SIMULATIONS

Similarly to dipole arrays, we simulated two-element and 3 by 3 patch antenna arrays to compare the performance of coupling compensation techniques. All patch antennas were modeled on a RG-5870 substrate with a relative permittivity of $\varepsilon_r = 2.33$ and a thickness of 20 mils. The antenna element is a rectangular patch with 37 mm (width) dimensions by 34 mm (length). The input impedance and the return loss for this antenna are shown in Figure 1 (a).

The first example involves a two-element array arranged along the E-plane (aligned with the resonant mode) with an inter-element spacing of 40 mm ($\sim 0.3\lambda$). HFSS was used to simulate three cases, and the results are presented in Figure 9. The scattering parameters (Figure 9 (d)) indicate that the mutual coupling between these two elements is -15.1 dB, which does not significantly affect the EEP of individual elements. Furthermore, the E-plane radiation pattern shows only a slight effect of mutual coupling (Figure 9 (e)). The VLT technique was subsequently applied, and the results were compared with both cases. As shown in Figure 9, the compensated array exhibits an additional pattern that is nearly indistinguishable from that of a single element.

In the second example, the two-element array was arranged along the H-plane. The simulations for the three cases are presented in Figure 10. Although mutual coupling is stronger in this configuration (Figure 10 (d)), the radiation patterns (Figure 10 (e)) demonstrate that the CCM effectively compensates for mutual coupling, restoring the pattern to match that of a single isolated element closely.

Finally, a 3×3 array of patch antennas was simulated with uniform spacing ($\sim 0.3\lambda$) along the x- and y-directions on a 200 mm $\times$ 200 mm ground plane. After simulating the array using HFSS, the CCM was computed as a function of frequency. An interesting observation is that the CCM elements exhibit significantly weaker frequency variation compared to the **Z**- and **S**-matrices (Figure 11). Also, the (ij) elements of the CCM are primarily influenced by the relative positions of elements i and j, with minimal impact from their absolute positions within the array. This property may assist in finding the matrix for larger arrays where measuring the impedance matrix is difficult.

We analyze the current distribution and radiation patterns when an antenna element in the 3×3 array is excited to further demonstrate the technique. Figure 12 shows the simulation results when the center element is excited for the three cases. Figures 12 (a, b, c) depict the current distribution for Cases 1, 2, and 3, demonstrating that the compensation technique effectively reduces the current in the surrounding elements to below -40 dB with respect to the excited element. This figure also shows that the VLT alters the reactive near-field of the antennas and nulls their current, indicating that it is not just a far-field modification. Figures 12 (d, e, f) show the simulated radiation patterns (magnitude and phase) in the E-plane ($\varphi = 0$) and H-plane ($\varphi = 90$). The results confirm that mutual coupling causes a significant distortion in the magnitude and phase of the electric field in both planes. In contrast, coupling compensation successfully restores the radiation pattern of the isolated element.

The last simulation involves the 3 by 3 array with element 1 (the corner element) excited (Figure 13). Comparison of Figures 13 (b) and 13 (c) shows that coupling compensation effectively reduces coupled currents on neighboring elements, resulting in radiation patterns almost identical to those of an isolated element (Figure 13 (d)). Despite the corner element's asymmetrical position on the ground plane, the compensated array maintains coherence in the radiated phase, with less than 1-degree phase variations.

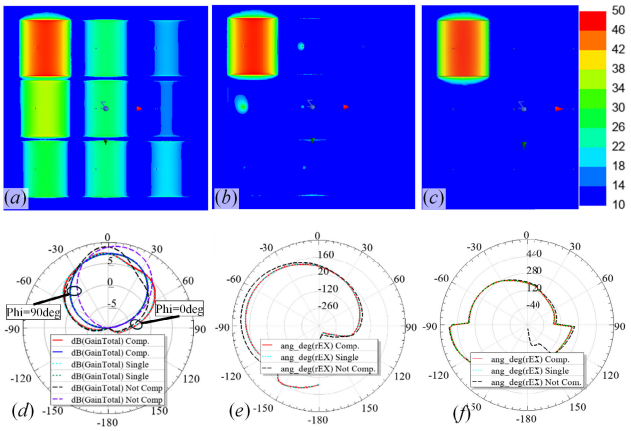

FIGURE 13. (a) Current distribution of the 9-element patch array with the corner element excited (Case 1). (b) Current distribution (Case 2). (c)Current distribution (Case 3). (d) E-plane and H-plane radiationpatterns for all three cases. (e) Phase of the co-polarized radiated field in the E-plane. (f) Phase of the co-polarized radiated field in the H-plane.

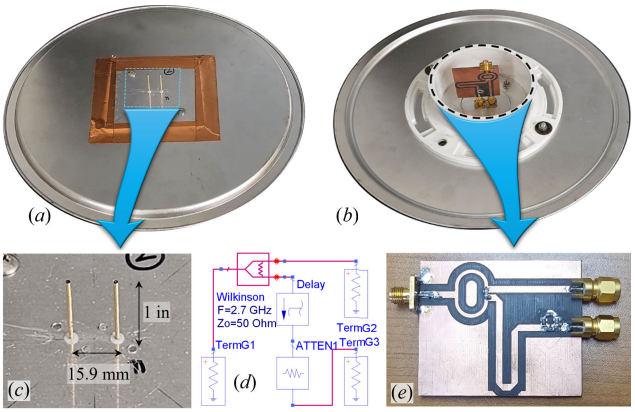

FIGURE 14. (a) Front view of the prototyped dipole array. (b) Rear view of the antenna array. (c) Monopole antennas. (d) Schematic of the feeding circuitry. (e) Feeding circuitry designed for precise magnitude and phase adjustment for radiating and compensated elements.

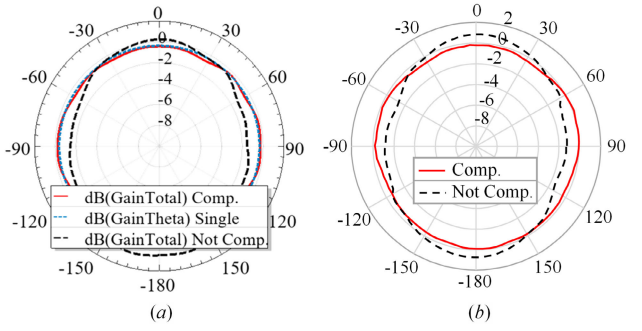

FIGURE 15. (a) Azimuth radiation pattern of the simulated monopole array. (b) Measured radiation pattern of the dipole array for compensated and non-compensated cases.

VI. MEASURED RESULTS

The two-element monopole array simulated in Section V was prototyped, as illustrated in Figure 14 (a and c). To implement coupling compensation, the input signal was split using a Wilkinson power divider. One portion of the signal fed the radiating element, while the other passed through a delay line and an attenuator to achieve the desired phase and amplitude characteristics determined from the simulations. A schematic of the feeding circuitry is shown in Figure 14 (d), and the physical feeding circuit is presented in Figure 14 (e). The feeding circuitry connected to the antenna array is depicted in Figure 14 (b).

Figure 15 (a) shows the simulation results for the radiation pattern in the azimuth plane across two scenarios: one element is excited through a matched source while the other is terminated to a 50Ω load (non-compensated), and the other curves display similar patterns when both elements are excited using coefficients derived from VLT (compensated array). Additionally, the simulation results for the case with only one element are included for comparison. Figure 15 (b) presents the measured radiation patterns for the antenna array depicted in Figure 14, where one element was excited with a coaxial cable while the other was terminated to a matched load. It also includes the measured results for the array when excited through the circuitry shown in Figure 14 (e). A single element monopole is expected to exhibit a circular radiation pattern in its azimuth plane; however, the presence of the second element disturbs the pattern due to mutual coupling. Consequently, this pattern is not circular. Nonetheless, we were able to reconstruct the circular pattern associated with a single element (zero mutual coupling with another element present) using VLT. Both figures demonstrate that the simulation and measured results validate the effectiveness of VLT, even for such a highly coupled antenna array.

VII. DISCUSSION AND CONCLUSION

In this study, we introduced a systematic approach to mitigating mutual coupling in antenna arrays using the generalized Virtual Load Theory (VLT). By analyzing the resonance characteristics of antenna elements and leveraging Thévenin-Helmholtz (TH) equivalent circuits, we developed an effective Coupling Compensation Matrix (CCM) to enhance Embedded Element Patterns (EEP) without requiring physical modifications.

Our simulations and experimental results confirm that VLT significantly reduces mutual coupling effects across various antenna configurations, ensuring improved beamforming accuracy and signal integrity. Notably, the open-circuit voltage/short circuit current ($\mathbf{V}_{oc}/\mathbf{I}_{sc}$)-based beamforming approach in the receiving arrays demonstrated resilience against coupling effects, establishing it as a dependable method for advanced antenna applications. Two important points are essential to the effectiveness of VLT: normalizing the CCM and de-embedding the parasitic elements.

Despite these advancements, challenges remain in obtaining accurate $\mathbf{Z}$ and $\mathbf{S}$ matrices in real-world environments, particularly for ultra-wideband and dynamically adaptive arrays. Future research should explore real-time adaptive tuning mechanisms within the signal processing domain to enhance the stability and efficiency of VLT in practical deployments.

This study's findings pave the way for more efficient antenna designs in communication, radar, and sensing systems. They address key limitations of conventional mutual coupling mitigation techniques.

ACKNOWLEDGMENT

The author thanks Shashank Chinnakkagari for his assistance in prototyping and measuring the monopole array. He also thanks the anonymous reviewers for their valuable comments and suggestions, which have greatly enhanced the quality of this article.

REFERENCES

[1] W. Amara, R. Ghayoula, A. Hammami, A. Smida, I. El Gmati, and J. Fattahi, "Phased array antenna controlled by FPGA-ARM Cortex-M processor," *Adv. Electromagn.*, vol. 12, no. 3, pp. 61–68, Oct. 2023.
[2] B. Bazuhair and O. Aldayel, "Fast antenna array calibration using one external receiver," *Sensors*, vol. 23, no. 22, p. 9026, Nov. 2023.
[3] M. de Kok, C. J. C. Vertegaal, A. B. Smolders, and U. Johannsen, "A 34- to 36-GHz active transmitarray for Ka-band tracking radar using 5G Tx/Rx beamforming ICs: Design and 64-element demonstrator," *IEEE Trans. Antennas Propag.*, vol. 71, no. 4, pp. 3260–3272, Apr. 2023.
[4] R. C. Hansen, *Microwave Scanning Antennas*. New York, NY, USA: Academic, 1966.
[5] R. J. Mailloux and F. J. Larussa, "A microwave phase bridge technique for measuring mutual coupling of identical coupled antennas," *IEEE Trans. Microw. Theory Techn.*, vol. 16, no. 2, pp. 129–137, Feb. 1968.
[6] R. J. Mailloux, "First-order solutions for mutual coupling between waveguides which propagate 2 orthogonal modes," *IEEE Trans. Antennas Propag.*, vol. 17, no. 6, pp. 740–745, Nov. 1969.
[7] S. Stein, "On cross coupling in multiple-beam antennas," *IRE Trans. Antennas Propag.*, vol. 10, no. 5, pp. 548–557, Sep. 1962.
[8] A. T. de Hoop, "A reciprocity theorem for the electromagnetic field scattered by an obstacle," *Appl. Sci. Res., Sect. B*, vol. 8, no. 1, pp. 135–140, Dec. 1960.
[9] A. T. de Hoop, "The n-port receiving antenna and its equivalent electrical network," *Philips Res. Rep.*, vol. 30, p. 13, Jan. 1975.
[10] D. Pinchera, J. W. Wallace, M. D. Migliore, and M. A. Jensen, "Experimental analysis of a wideband adaptive-MIMO antenna," *IEEE Trans. Antennas Propag.*, vol. 56, no. 3, pp. 908–913, Mar. 2008.
[11] K. Yang, Z. Zhao, Z. Nie, J. Ouyang, and Q. H. Liu, "Synthesis of conformal phased arrays with embedded element pattern decomposition," *IEEE Trans. Antennas Propag.*, vol. 59, no. 8, pp. 2882–2888, Aug. 2011.
[12] D. F. Kelley, "Embedded element patterns and mutual impedance matrices in the terminated phased array environment," in *Proc. IEEE Antennas Propag. Soc. Int. Symp.*, vol. 3A, Jul. 2005, pp. 659–662.
[13] P. S. Kildal and K. Rosengren, "Electromagnetic characterization of MIMO antennas including coupling using classical embedded element pattern and radiation efficiency," in *Proc. IEEE Antennas Propag. Soc. Symp.*, vol. 2, Jun. 2004, pp. 1259–1262.
[14] K. F. Warnick, D. B. Davidson, and D. Buck, "Embedded element pattern loading condition transformations for phased array modeling," *IEEE Trans. Antennas Propag.*, vol. 69, no. 3, pp. 1769–1774, Mar. 2021.
[15] C. Pfeiffer, F. Dagefu, B. Tomasic, J. N. Twigg, and B.-I. Wu, "Virtual impedance method for mutual coupling compensation," *IEEE Trans. Antennas Propag.*, vol. 69, no. 8, pp. 4569–4579, Aug. 2021.
[16] B. Strait and K. Hirasawa, "Array design for a specified pattern by matrix methods," *IEEE Trans. Antennas Propag.*, vol. AP-17, no. 2, pp. 237–239, Mar. 1969.
[17] N. Inagaki, T. Sekiguchi, and K. Nagai, "Exact design of an array of dipole antennas giving the prescribed radiation patterns," *IEEE Trans. Antennas Propag.*, vol. AP-19, no. 1, pp. 128–129, Jan. 1971.
[18] A. U. Zaman, M. Alexanderson, T. Vukusic, and P.-S. Kildal, "Gap waveguide PMC packaging for improved isolation of circuit components in high-frequency microwave modules," *IEEE Trans. Compon., Packag., Manuf. Technol.*, vol. 4, no. 1, pp. 16–25, Jan. 2014.
[19] F. Yang and Y. Rahmat-Samii, "Microstrip antennas integrated with electromagnetic band-gap (EBG) structures: A low mutual coupling design for array applications," *IEEE Trans. Antennas Propag.*, vol. 51, no. 10, pp. 2936–2946, Oct. 2003.
[20] D. Liu, J. Hirokawa, J. R. Costa, C. A. Fernandes, and R. Sauleau, "Guest editorial for the special issue on antennas and propagation at mm- and sub mm-waves," *IEEE Trans. Antennas Propag.*, vol. 61, no. 4, pp. 1502–1507, Apr. 2013.
[21] Y. Zhang, J. Bai, S. Shi, and D. W. Prather, "Ka-band phased patch array antenna integrated with a PET-controlled phase shifter," *Int. J. RF Microw. Comput.-Aided Eng.*, vol. 26, no. 3, pp. 199–208, Mar. 2016.
[22] Z. Li, Z. Du, M. Takahashi, K. Saito, and K. Ito, "Reducing mutual coupling of mimo antennas with parasitic elements for mobile terminals," *IEEE Trans. Antennas Propag.*, vol. 60, no. 2, pp. 473–481, Feb. 2012.
[23] D. Guha, M. Biswas, and Y. M. M. Antar, "Microstrip patch antenna with defected ground structure for cross polarization suppression," *IEEE Antennas Wireless Propag. Lett.*, vol. 4, pp. 455–458, 2005.
[24] M. S. Sharawi, A. T. Hassan, and M. U. Khan, "Mutual coupling reduction in compact mimo antenna operating over ultra-wideband application," *IET Microw., Antennas Propag.*, vol. 9, no. 8, pp. 826–832, 2015.
[25] X. Chen, S. Zhang, and Q. Li, "A review of mutual coupling in mimo systems," *IEEE Access*, vol. 6, pp. 24 706–24719, Apr. 2018.
[26] S. Henault and Y. Antar, "Unifying the theory of mutual coupling compensation in antenna arrays," *IEEE Antennas Propag. Mag.*, vol. 57, no. 2, pp. 104–122, Apr. 2015.
[27] I. Gupta and A. Ksienski, "Effect of mutual coupling on the performance of adaptive arrays," *IEEE Trans. Antennas Propag.*, vol. AP-31, no. 5, pp. 785–791, Sep. 1983.
[28] H. Steyskal and J. S. Herd, "Mutual coupling compensation in small array antennas," *IEEE Trans. Antennas Propag.*, vol. 38, no. 12, pp. 1971–1975, Aug. 1990.
[29] D. M. Pozar, "The active element pattern," *IEEE Trans. Antennas Propag.*, vol. 42, no. 8, pp. 1176–1178, Aug. 1994.
[30] C. Craeye and D. González-Ovejero, "A review on array mutual coupling analysis," *Radio Sci.*, vol. 46, no. 2, pp. 1–25, Apr. 2011.
[31] H.-S. Lui, H. T. Hui, and M. Seng Leong, "A note on the mutual-coupling problems in transmitting and receiving antenna arrays," *IEEE Antennas Propag. Mag.*, vol. 51, no. 5, pp. 171–176, Oct. 2009.
[32] S. A. Schelkunoff, "Some equivalence theorems of electromagnetics and their application to radiation problems," *Bell Syst. Tech. J.*, vol. 15, no. 1, pp. 92–112, Jan. 1936.
[33] S. A. Schelkunoff, "Kirchhoof's formula, its vector analogue, and other field equivalence theorems," *Commun. Pure Appl. Math.*, vol. 4, no. 1, pp. 43–59, Jun. 1951.
[34] R. E. Collin, *Foundations for Microwave Engineering*. New York, NY, USA: Wiley, 2000.
[35] M. Manteghi, "Generalized scattering matrix formulation and its relationship with TARC and maximum power transfer theorem," 2024, *arXiv:2412.13308*.

MAJID MANTEGHI (Senior Member, IEEE) received the B.S. and M.S. degrees in electrical engineering from the University of Tehran, Tehran, Iran, in 1994 and 1997, respectively, and the Ph.D. degree in electrical engineering from the University of California at Los Angeles (UCLA), Los Angeles, CA, USA, in 2005.

From 1997 to 2000, he worked in the telecommunications industry in Tehran, where he led the RF Team for a GSM Base Transceiver Station Project. In 2000, he joined the Antenna Research, Analysis, and Measurement Laboratory, UCLA. After receiving the Ph.D. degree, he continued as a Lecturer with the Department of Electrical Engineering, UCLA, and was a Research Scientist with Mojix Inc., Los Angeles. Since 2007, he has been a Faculty Member with Virginia Tech Antenna Group and The Bradley Department of Electrical and Computer Engineering, Virginia Polytechnic Institute and State University (Virginia Tech), Blacksburg, VA, USA. His research interests include non-linear time-variant techniques in antennas and microwave devices, electrically small antennas, chipless RFID, singularity expansion method (SEM)-based space-time-frequency detection techniques, wireless power transfer, implanted antennas, intra- and interbody wireless components and systems, ultrawideband (UWB) impulse-radiating antennas (IRAs), phased array design, multiport antennas, and remote antenna measurements.